Session 2.4 Linking Weather and Climate

Coupling of water vapor convergence, clouds, precipitation and land-surface processes in the climate over land

Alan K. Betts
Atmospheric Research,
Pittsford, VT 05763

akbetts@aol.com

November 1, 2006

(Preprint)

Abstract

On daily time-scales, the climate over land is a complex balance of many coupled processes. ERA40 reanalysis data for sub-basins of the Mississippi in summer are used to explore the links between these processes in a fully coupled model system; and observed surface precipitation and surface shortwave fluxes derived by the International Satellite Cloud Climatology Project are used for evaluation. This paper proposes that the effective cloud albedo at the surface is a useful link which connects the cloud fields to both surface and large-scale processes. The reanalysis has a low bias in cloud albedo in all seasons except summer. Near-surface relative humidity, the lifting condensation level, soil moisture and precipitation are closely linked. The ratio of the surface cloud radiative forcing to the diabatic precipitation heating is less in the reanalysis than in the observations. The surface cloud radiative forcing largely determines the surface net radiation; while evaporative fraction in the reanalysis is primarily determined by temperature, soil water as well as vegetation parameters.

1. Introduction

On time-scales of a day and space scales of order 800km, the climate over land is a complex balance of many highly coupled processes. In the atmosphere, water vapor convergence is linked to precipitation and clouds, which in turn modify the radiation fields. Over land the surface energy budget is strongly influenced by the cloud field, and the availability of water for evaporation. Reanalysis data for sub-basins of the Mississippi will be used to explore the links between these processes on river basin scales, using for evaluation observed surface precipitation and surface shortwave fluxes derived by the International Satellite Cloud Climatology Project (ISCCP). For more than a decade, cloud feedbacks in models have been regarded as a major source of uncertainty in modeling climate. Clouds play a major role in the climate system through their top-of-the-atmosphere (TOA) impact of the radiative fluxes, where they increase the planetary albedo and typically reduce the outgoing long-wave flux. Yet the TOA radiative effects of clouds are easy to observe from space, and the surface radiative fluxes are routinely derived from them [*Pinker et al.* 2003]. So given this extensive observational data, which clearly identifies model biases in the surface radiation budget [e.g. *Betts et al.* 2006b], why haven't corresponding improvements in models been rapid? This paper proposes that the effective cloud albedo at the surface is one missing observable link that can be used to connect the cloud fields to both surface and large-scale processes. The cloud fields are a tightly coupled component of the hydrologic cycle and the climate system. Over land, clouds are partly linked locally to the availability of soil water, which impacts evaporation and the lifting condensation level (LCL); and partly linked to large-scale convergence of moisture which generates clouds and precipitation. The system is tightly coupled at the surface because clouds reduce the incoming short-wave and outgoing long-wave radiative fluxes, which generally reduces the energy available to drive evaporation. In addition, some precipitation evaporates as it falls

(modifying atmospheric properties including the LCL), some precipitation evaporates rapidly off wet canopies, while some refills the soil water reservoirs (and some runs off). From a climate and energetic perspective, the relation between the precipitation diabatic forcing of the atmosphere and the surface cloud radiative forcing is important.

Betts [2004] and *Betts and Viterbo* [2005] used reanalysis data to explore the interrelation of the surface fluxes, the boundary layer, the cloud fields and surface radiation balance on the daily timescale. This paper extends this work to the coupling of water vapor convergence, clouds, precipitation and land-surface processes for the mid-latitude basins of the Mississippi River. The European Centre for Medium-range Weather Forecasts (ECMWF) reanalysis [*Uppala et al.* 2005] is known as ERA40, although it covered 45 years from September, 1957 to August, 2002. It used the land-surface scheme described by *Van den Hurk et al.* [2000], and a 3-D variational assimilation system. The horizontal resolution of the spectral model is triangular truncation at T_L-159, and there are 60 levels in the vertical, including a well-resolved boundary layer and stratosphere. Documentation of the Integrated Forecast System (IFS), cycle 23r4, and a summary and discussion of the observations available at different times during the 45-year reanalysis can be found at http://www.ecmwf.int/research/era/. One feature of ERA40 is a special hourly archive [*Källberg, et al.* 2004] of averages over selected river basins (accumulated from the full time resolution data) of the surface energy and water budgets, as well as the sub-surface, near-surface and atmospheric variables. These were originally archived to study the hydrometeorology of river basins [for example, *Betts et al.* 2003a, b; 2005]. However model data can provide powerful insights into the coupling of physical processes, even though quantitatively there will be dependence on specific parameterizations of a given model [*Betts* 2004, 2006]. The organization of model data by the effective cloud albedo at the surface clarifies the links between processes, and provides a useful

framework for model evaluation against surface flux tower data [*Betts et al.* 2006a]. This paper extends this evaluation of cloud albedo and precipitation to river basin scales. Finally the coupling of model processes involving clouds, precipitation and the surface energy budget suggests how combinations of satellite data and surface variables may give better estimates of the surface energy budget.

2. Data and definitions

2.1 Mississippi basin data from ERA40

Figure 1 shows the sub-basins of the Mississippi river, labeled 1 to 5, representing respectively the Red-Arkansas, the Missouri, Upper Mississippi, Ohio-Tennessee, and the lower Mississippi. During the analysis cycle ERA40 generated averages over all grid-points (indicated as dots) inside each polygon, which are approximations to the actual river basin boundaries shown. The data period chosen for analysis is from 1983-2001, for which there is ISCCP data for comparison. Daily means were derived for each basin by averaging the hourly data from a single 24-h short-term forecasts from the 0000 UTC analysis. The annual cycle of precipitation and cloud for the basins labeled 1 to 4 will be shown. The analysis will then concentrate on the warm season for only two basins, the Missouri (area of 1.3 x10^6 km^2) and Ohio (area of 0.46 x10^6 km^2), taking these as

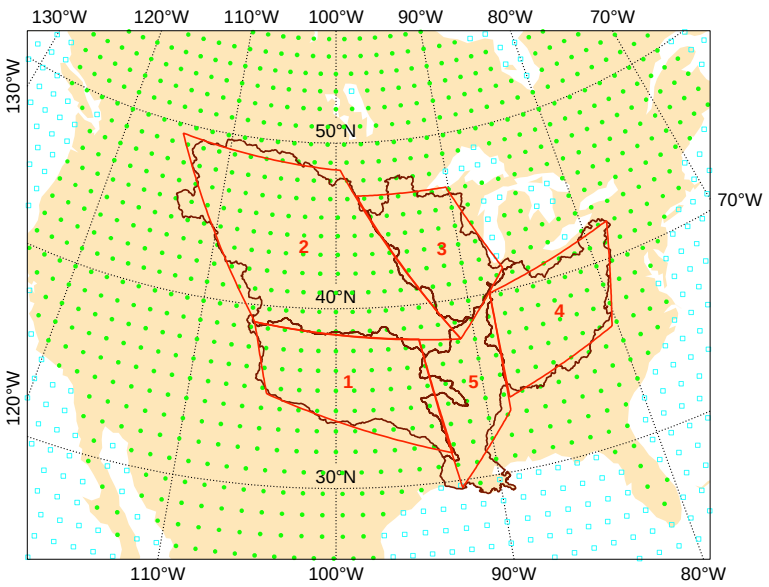

Figure 1. ERA40 river basins for the Mississippi river.

representative of the drier central and the wetter eastern United States respectively. The advection distance in 24-h at 10 ms^{-1} is 864 km. This corresponds to roughly 10^o of longitude at 40^oN, which roughly lies between the spacial scales of the Ohio and Missouri river basins (see Figure 1). There are differences in the model vegetation between the two basins; the Ohio is over 85% forested, while the Missouri forest cover is less than 15%.

2.2 Definition of effective surface cloud albedo

The ERA40 archive [*Kållberg et al.*, 2004] contains net 'clear-sky' fluxes (surface, SRF, and top-of-the-atmosphere, TOA) computed without the model cloud field, as well as the radiation fluxes computed with the model (prognostic) cloud field. The cloud forcing (CF) terms can be computed from these net SW and LW fluxes by difference. At the surface, the shortwave cloud forcing is defined as the difference of the surface net short-wave all-sky and clear sky fluxes

$$SWCF_{SRF} = SW_{netSRF} - SW_{netSRF}(clear) \quad (1)$$

and the surface effective cloud albedo as

$$\alpha_{cloud} = - SWCF_{SRF}/SW_{netSRF}(clear) \quad (2)$$

so that the SW surface budget can be written in the symmetric form

$$SW_{netSRF} = (1- \alpha_s)(1- \alpha_{cloud}) SW_{dnSRF}(clear) \quad (3)$$

where SW_{dnSRF} is the downward SW flux at the surface. The albedo of the underlying surface, α_s, (assumed the same for both the clear-sky and all-sky fluxes) satisfies both

$$\alpha_s = (SW_{dnSRF} - SW_{netSRF})/SW_{dnSRF}$$
$$= (SW_{dnSRF}(clear) - SW_{netSRF}(clear))/SW_{dnSRF}(clear) \quad (4)$$

The total cloud forcing at the surface is

$$CF_{SRF} = SWCF_{SRF} + LWCF_{SRF} \quad (5)$$

where the LW cloud forcing is defined in a similar manner as

$$LWCF_{SRF} = LW_{netSRF} - LW_{netSRF}(clear) \quad (6)$$

The transformation represented by (1) and (2) is illustrated in Figure 2 for five years of daily mean data for the Ohio river basin. The upper panel shows SW_{net}, as a distribution of scattered points below $SW_{netSRF}(clear)$, which form an upper envelope. The difference, $SW_{netSRF} - SW_{netSRF}(clear)$ is the SW cloud forcing given by (1) and it is always negative. The lower panel shows the effective cloud albedo from (2), which always satisfies $0 < \alpha_{cloud} < 1$. This transformation removes the large seasonal variation of clear-sky fluxes associated with changing solar zenith angle. The range of effective cloud albedo is greater in winter than in summer for this basin. α_{cloud} is an "effective" surface cloud albedo, because it represents the fraction of the clear sky flux that does not reach the surface because of the cloud field. Thus it includes both the reflection and the smaller absorption by the cloud field. For brevity however it will be simply called surface cloud albedo.

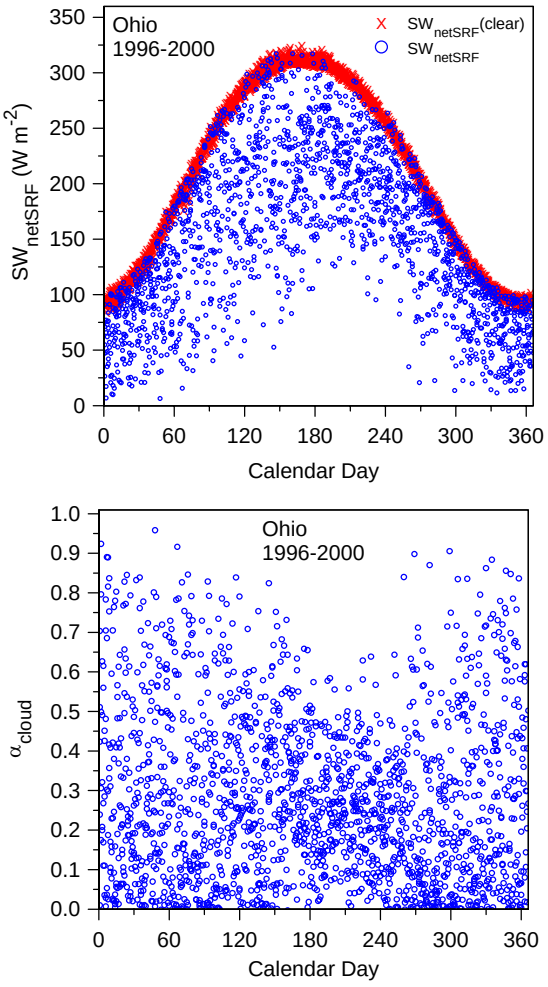

Figure 2. Annual distribution of total and clear sky SW_{netSRF} (upper panel) and effective surface cloud albedo (lower panel).

2.3 Relation of surface and TOA cloud albedos

The TOA cloud albedo is related to the TOA cloud forcing by

$$\alpha_{TOA} = - SWCF_{TOA}/SW_{dnTOA}(clear) \quad (7)$$

where the TOA SW cloud forcing is defined as

$SWCF_{TOA} = SW_{netTOA} - SW_{netTOA}(clear)$ (8)

Figure 3 shows the relation of the TOA cloud albedo from (7) to the effective surface cloud albedo, defined by (2). The daily mean data have been binned by α_{TOA} and by warm and cold seasons. For visual reference, a quadratic relationship

$\alpha_{cloud} = 1.8\ \alpha_{TOA} + 0.25\ \alpha_{TOA}^2$ (9)

is plotted as a heavy dashed line. In ERA40, the relationship between TOA and effective surface cloud albedos varies only a little by season and between river basins (not shown). Note also that the standard deviations of the daily data, averaged over the Ohio basin, while small, are a little larger in the cold season, when the clear-sky solar fluxes are smaller. These cloud albedos are useful quantitative measures of the cloud field. In this section, they are derived from the model cloud fields, but they are also readily derived from satellite data (see next section).

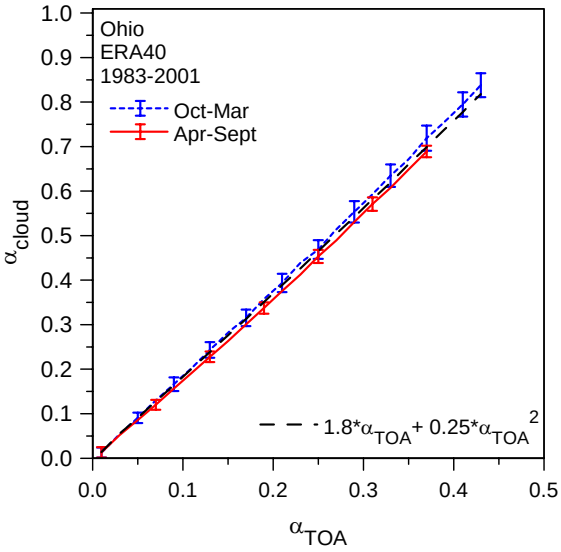

Figure 3. Relation of surface and TOA cloud albedos.

2.4 Evaluation data

Two sets of observationally based data are used for verification. 'Observed' surface cloud albedos were derived from the daily means of the ISCCP SW_{dnSRF} fluxes [*Zhang et al.* 1995; *Rossow and Zhang* 1995] averaged over the Mississippi basins [see *Betts et al.*, 2003a] using the ERA40 $SW_{dnSRF}(clear)$. The ISCCP computed surface LW fluxes will not be used, as these are sensitive to errors in surface temperature and lower tropospheric temperature profiles [*Betts et al.* 2003a]. For

precipitation, the 2 x 2.5 degree gridded hourly [*Higgins et al.* 1996] and 0.25 degree gridded daily [*Higgins et al.* 2000] products from the National Climatic Data Center (NCDC) were averaged over the Mississippi sub-basins. The daily product uses many more rain-gages than the hourly product, and has greater precipitation in all seasons. However, the 'day' starts and ends at 1200UTC, (when most of the daily gages are read), whereas in all our other analyses the day runs from 0000-2400 UTC. So a daily mean was derived from the hourly data and then the precipitation was scaled upward with a smoothed monthly weighting function to match the monthly mean from the gridded daily product.

3. ERA40 seasonal bias of cloud and precipitation

3.1 ERA40 cloud albedo bias

The upper curves in Figure 4 shows the mean seasonal cycle of this ISCCP-derived cloud albedo for four Mississippi sub-basins. The lower curves are the ERA40 α_{cloud} bias, defined as α_{cloud}(ERA40) - α_{cloud}(ISCCP). ERA40 has a systematic bias structure with too little reflective cloud except in summer. This albedo bias in the reanalysis is as large as -10% in winter. A representative set of standard deviations of the monthly means are shown for one basin: note that typically the variability of the model bias is less than the interannual variability of the observed cloud albedo. This seasonal bias pattern in cloud albedo is very similar to that found in a comparison study [*Betts et al.*

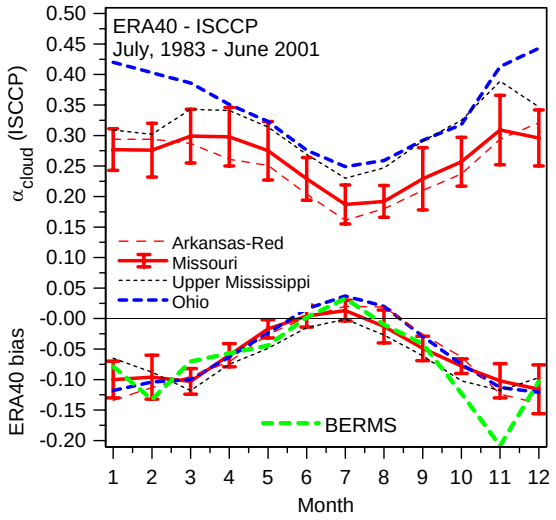

Figure 4. Mean seasonal cycle of ISCCP surface cloud albedo and ERA40 bias. The bias against BERMS flux tower sites is also shown.

2006a] with the three Boreal Ecosystem Monitoring Study (BERMS) flux tower sites in central Saskatchewan, which is shown in green.

Figure 5 shows the distribution of days with a given cloud albedo in (a) winter and in (b) summer for the ISCCP data, and the bias, ERA40-ISCCP. In winter ERA40 has many more days with very little cloud and many fewer days in every cloud albedo class > 0.2. This pattern suggests that ERA40 underestimates cloud cover (see Figure 6). In summer, the ERA40 bias pattern is smaller; and the ISCCP distributions are more peaked in the range 0.1-0.2, with generally fewer clear days than ERA40.

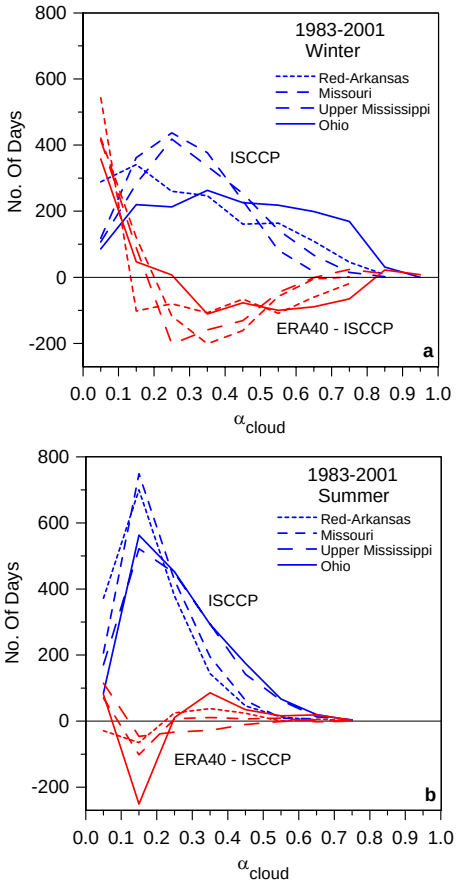

Figure 5. Number of days with a given cloud albedo (a) in winter and (b) in summer for the ISCCP data, and the ERA40 bias.

3.2 Daily scatterplots of albedo bias

Figure 6 compares daily ERA40 cloud albedo with ISCCP for the Ohio basin for the four seasons (winter is December, January, February etc). The scatter between observations and reanalysis is relatively small on the daily timescale, only ± 0.1, but the systematic seasonal biases are clearly visible. In winter, ERA40 has a low cloud bias on almost all days, except when it is very cloudy. The bias is smaller in spring and fall, while in summer there is a small high bias, as shown in Figure 4.

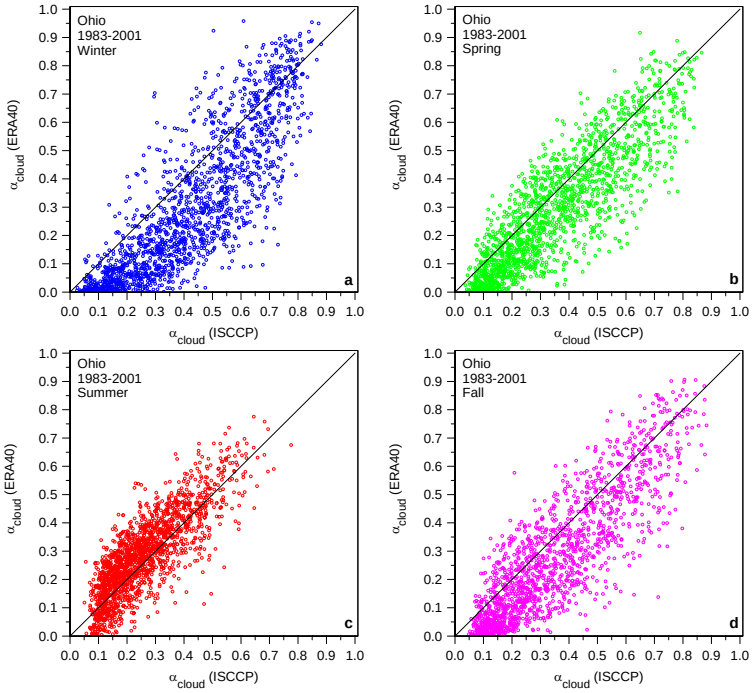

Figure 6. Scatterplot of daily mean cloud albedo for ERA40 against ISCCP for Ohio river basin for winter, spring, summer and fall.

3.3 ERA40 precipitation bias

Figure 7 shows the annual cycle of the observed NCDC precipitation and the bias, ERA40 - NCDC. The standard deviations of the monthly means shown for the Missouri river basin are typical: note that the interannual variability of precipitation is larger than the variability of the bias. The reanalysis precipitation bias for most basins is weakly positive in winter. In summer, the Ohio basin (and the lower Mississippi, not shown) has a high precipitation bias quite different from the other three basins. Comparing Figures 4, 6 and 7 it is clear that in winter ERA40 has too low a cloud albedo, but generally a positive precipitation bias. This clearly suggests that the large-scale precipitation process in the model, which is dominant in winter, is too efficient in its removal of cloud water. One caveat is that during the first 24 h of the ERA40 short term forecasts, while cloud albedo changes little, the spinup of precipitation is considerable [*Betts et al.* 2003a].

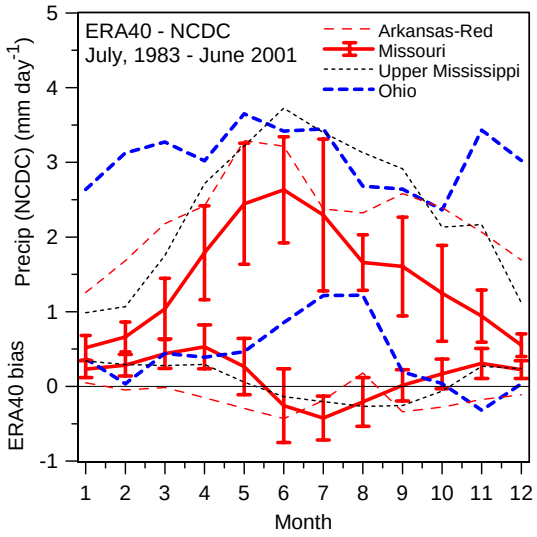

Figure 7. Mean seasonal cycle of NCDC precipitation and ERA40 bias.

4. Warm season links between moisture convergence, cloud and precipitation

4.1 Analysis strategy

The model bias in cloud albedo is small (Figure 4) in the warm season months, May-August, when land-surface processes play an important role in the land-boundary-layer-atmosphere coupling [*Betts et al.* 1996]. The model dataset was analyzed, looking for relationships between

key surface variables, precipitation, CF_{SRF}, and evaporative fraction, EF, and α_{cloud} as a measure of the cloud field. The daily basin averaged from the ISCCP data and precipitation from the NCDC data were used for evaluation.

Three parameters were taken from the reanalysis to additionally stratify the data. Large-scale forcing was represented quantitatively by the daily mean vertically integrated moisture convergence, VIMC, for each basin, generated from the four analysis times. Moisture convergence clearly generates clouds and precipitation. A soil moisture index was computed for the first 0-7cm soil layer as

$$\text{SMI-L1} = (\text{SM} - 0.171)/(0.323-0.171) \qquad (10)$$

where SM is the model soil water fraction, the model soil permanent wilting point is 0.171 and the model field capacity is 0.323. SMI-L1 is not only a useful index on the daily timescale for the availability of water for evaporation (although transpiration depends also on soil water in deeper layers), but it also responds to precipitation on this timescale. Thus, the soil moisture-atmosphere coupling is a two-way interaction. In addition the evaporation of falling precipitation modifies the boundary layer. The surface evaporative fraction (EF) depends on soil water, as well as water in the skin reservoirs, and in turn the EF modifies the boundary layer structure and boundary layer cloud cover. As an indicator of the boundary layer equilibrium on daily timescales [see *Betts* 2004], and an estimate of the mean height of cloud-base, the height of the lifting condensation level (LCL) in pressure coordinates, P_{LCL},, was computed from the lowest model level data (about 10m above the surface). P_{LCL} is closely related to near-surface relative humidity, RH, by the formula [*Betts*, 1997]

$$P_{LCL}/p = (1-RH)/(A+(A-1)RH) \qquad (11)$$

where p is the pressure at this lowest model level (about 1hPa from the surface) and the

thermodynamic coefficient $A = (0.622L/2C_pT)$ is a weak function of Kelvin temperature, T, with L being the latent heat of vaporization and C_p the specific heat of air at constant pressure.

4.2 Relationship of cloud albedo and precipitation to moisture convergence and cloud-base

Figure 8 shows the relation of the surface cloud albedo in ERA40 (panels (a) and (c)) and the ISCCP data (panels (b) and (d)) for the Missouri and Ohio basins, stratified by the two model quantities: vertically integrated moisture convergence, VIMC (bins of 5 mm day^{-1}), and P_{LCL} (40 hPa bins), an estimate of the daily mean cloud base. Not surprisingly, α_{cloud} increases with moisture convergence and a lower cloud base. Observed and model distributions are rather similar, especially for the western Missouri basin. In general, the spread in the ISCCP cloud albedo is lower than in ERA40. The representative standard deviations shown are smaller for the Missouri basin, which has about three times the area of the Ohio basin. Since α_{cloud} is derived from the incoming surface shortwave radiation from completely independent sources, the general agreement in Figure 8 is encouraging.

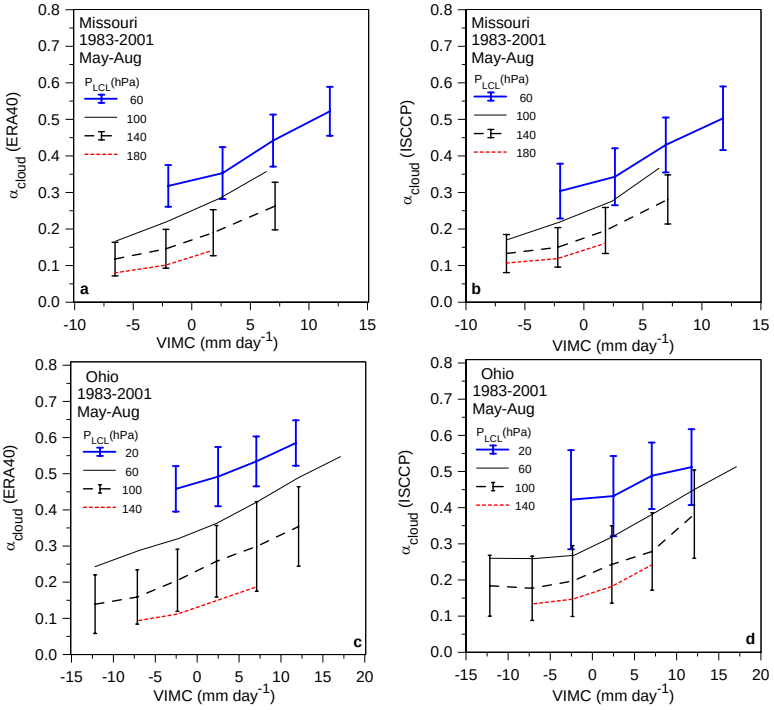

Figure 8. ERA40 and ISCCP cloud albedos as a function of moisture convergence and P_{LCL}.

Figure 9 shows that ERA40 and NCDC precipitation for the same river basins also increases with moisture convergence and decreasing cloud base. Indeed the ERA40 pattern for

cloud albedo in Figure 8 and precipitation in Figure 9 are somewhat similar. As cloud-base lowers, the slope of precipitation with moisture convergence becomes steeper. The spread however in precipitation is a little less in the NCDC data than in ERA40, and the greater precipitation for the Ohio basin in ERA40 is apparent.

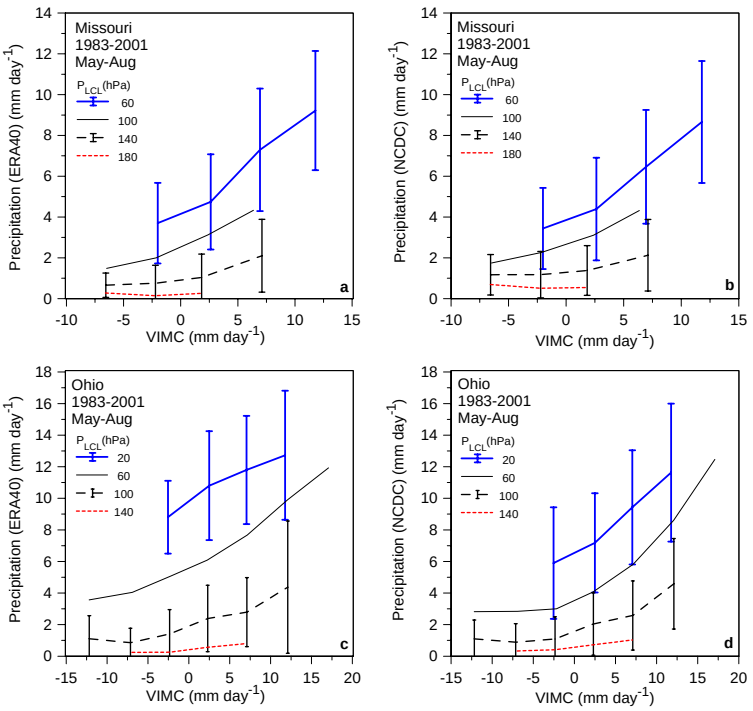

Figure 9. ERA40 and NCDC precipitation as a function of moisture convergence and P_{LCL}.

4.3 ERA40 soil moisture relations

There is no data to evaluate model soil moisture on the basin scale, but the internal relations in ERA40 are of interest.

4.3.1 Dependence of cloud and precipitation on soil moisture

Figure 10 shows the relationship between ERA40 soil moisture index for the first 0-7cm layer and α_{cloud} and precipitation (in mm day^{-1}), sub-divided into four 5 mm day^{-1} ranges of VIMC from a divergence of -7.5 mm day^{-1} to 7.5 mm day^{-1} moisture convergence. The upper panels are for the Missouri and the lower pair for the Ohio

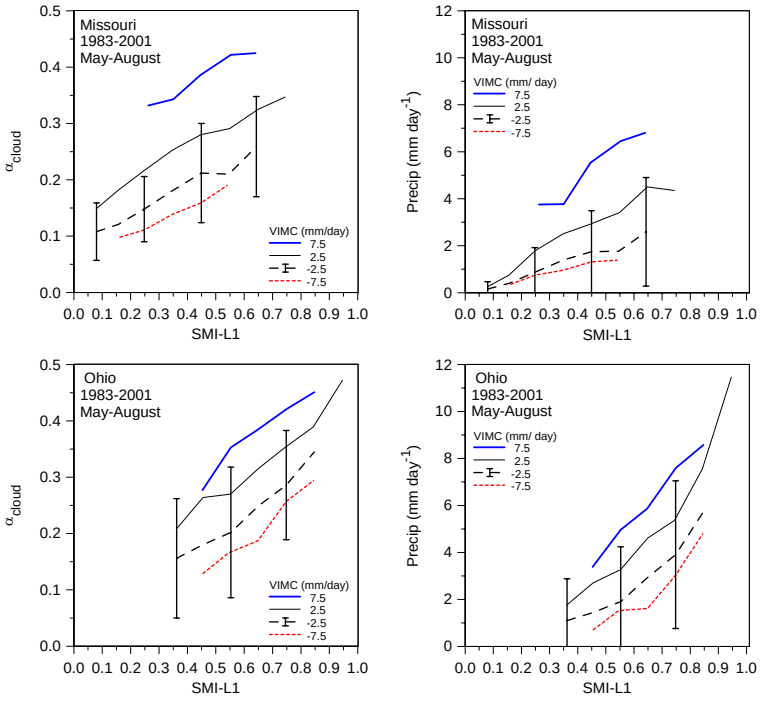

Figure 10. ERA40 α_{cloud} and precipitation dependence on soil moisture index, stratified by VIMC.

river. Cloud albedo and precipitation both increase with SMI-L1 and VIMC. Standard deviations are generally higher for the Ohio (a representative set are shown). The distributions are generally similar, but are shifted towards higher soil water, cloud cover and precipitation for the generally wetter Ohio basin. Indeed the Ohio has a substantial number of days with VIMC > 10 mm day^{-1}.

4.3.2 Soil moisture, lifting condensation level, RH and precipitation links

Figure 11 shows the link between soil moisture index, P_{LCL}, stratified by daily precipitation rate (PR) in five classes:

PR < 1 mm day^{-1}, labeled 0.5

1 < PR < 2 mm day^{-1}, labeled 1.5

2 < PR < 4 mm day^{-1}, labeled 3

4 < PR < 8 mm day^{-1}, labeled 6

PR > 8 mm day^{-1}, labeled 12

Near-surface RH is shown (with slight approximation) on the right-hand-scale. LCL decreases and RH increases as SMI and precipitation increase, and the relationships are similar for both basins. The soil moisture-atmosphere coupling is a two-way interaction. Soil moisture, especially in the upper soil layer responds directly to precipitation. Evaporation from the surface increases with increasing soil moisture (as well as when there is water in the skin reservoir) and this increases RH and lowers the LCL. In addition the evaporation of falling precipitation lowers the

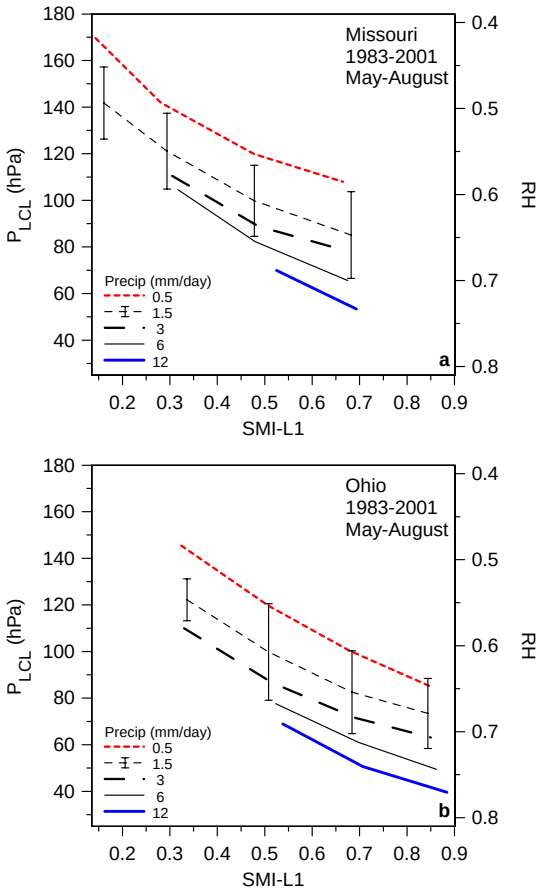

Figure 11. Link between soil moisture index, P_{LCL}, and RH, stratified by daily precipitation rate.

LCL by bringing the sub-cloud layer closer to saturation, and this effect increases with increasing precipitation rate. These relationships are largely independent of temperature.

4.4 Stratification of precipitation by cloud albedo and P_{LCL}

Figures 8, 9 and 10 show similar dependencies for precipitation and cloud albedo. Figure 12 shows that the relation of precipitation to cloud albedo is similar increase for both model and observations, and little dependence on moisture convergence can be seen, within the standard deviations shown for the daily data.

Figure 13 further sub-divides the data by reanalysis P_{LCL}. Greater precipitation is linked to both greater α_{cloud} and lower mean LCL. For the Missouri basin, the variation of observed precipitation with observed cloud albedo

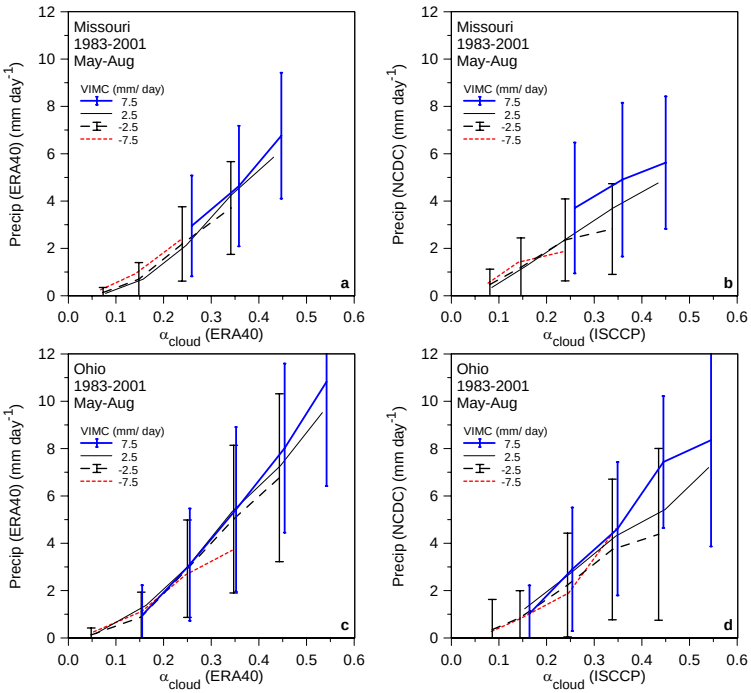

Figure 12. Relation between precipitation and cloud albedo, stratified by VIMC for ERA40 (left) and for observations (right).

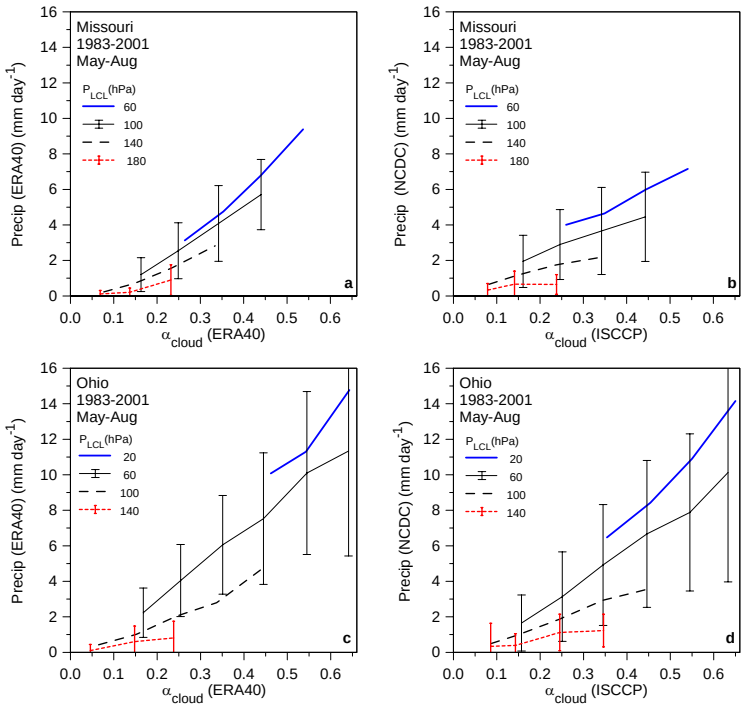

Figure 13. Relation between precipitation and cloud albedo, stratified by P_{LCL} for ERA40 (left) and for observations (right).

is noticeably less steep than the corresponding relation in ERA40. This increases the ratio of the surface cloud radiative forcing to the diabatic precipitation forcing (see Figure 15 later). The coupling of precipitation with LCL goes both ways, as discussed in section 4.3.2. A lower LCL is associated with a higher saturation mixing ratio at cloud base (and therefore more precipitation, and the evaporation of falling precipitation lowers the LCL. Nonetheless, this means that knowledge of the near-surface LCL provides additional information in the determination of say precipitation from satellite radiances.

4.5 Links between cloud albedo, cloud radiative forcing, cloud-base and precipitation

The relationship between the surface cloud radiative forcing and the diabatic forcing of the atmosphere by precipitation heating is a fundamental importance to the land-surface-atmosphere coupling. There are longwave and shortwave components to the cloud radiative forcing. The longwave cloud forcing depends on atmospheric temperature and moisture structure as well as the cloud field. Figure 14(a) shows the relationship between daily mean P_{LCL}, the mean clear-sky LW_{netSRF}(clear) and the surface all-sky LW_{netSRF}, stratified by cloud albedo. In ERA40, LW_{netSRF}(clear), the lowest curve, varies with the LCL, which is related to the low-level RH through (11). A higher mean cloud-base gives a

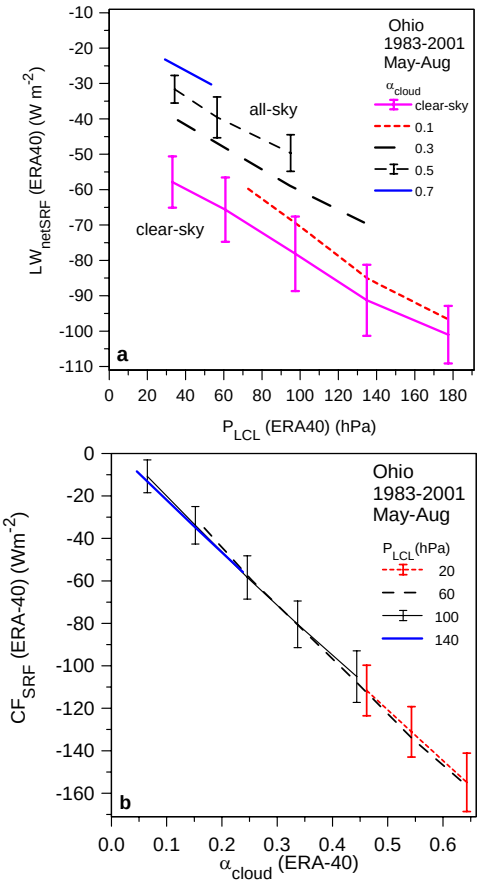

Figure 14. (a) Relation of all-sky and clear-sky LW_{netSRF} to P_{LCL} and α_{cloud}, (b) Surface cloud forcing dependence on α_{cloud} and P_{LCL}.

larger outgoing LW_{netSRF}(clear). The outgoing all-sky LW_{netSRF} (upper curves) decreases further with increasing α_{cloud}. The $LWCF_{SRF}$, defined by (6) as the difference varies primarily with α_{cloud}. As a result, the surface total cloud forcing, CF_{SRF} shown in Figure 14(b), is almost a linear function of α_{cloud} with no dependence on LCL. The Missouri basin is similar (not shown), except that for the same α_{cloud}, CF_{SRF} is a little smaller in magnitude for the Missouri. There are two reasons for this: the Missouri basin has a higher mean latitude, so that the mean SW fluxes are a little smaller, and the atmosphere over the Missouri is drier, so that the outgoing net LW fluxes are a little larger in magnitude. The ISCCP surface LW fluxes are not good enough to evaluate the LW cloud forcing in ERA40 [Betts et al. 2003a]. However, the short wave component is a linear function of α_{cloud} through (2), so the relation of the surface SW forcing to precipitation in the reanalysis can be evaluated with the ISCCP data.

Figure 15 takes the stratification by α_{cloud}. and P_{LCL} from Figure 13 and remaps to show the relationship of precipitation diabatic heating (in Wm^{-2}) to the surface SW cloud forcing. ERA40 is on the left for the Missouri and Ohio basins and on the right is the corresponding relation between the NCDC precipitation and the ISCCP cloud forcing. The relationships are similar for both basins, with slightly larger cloud-forcing for the Ohio, when cloud cover and precipitation is high, as discussed above. For the Ohio,

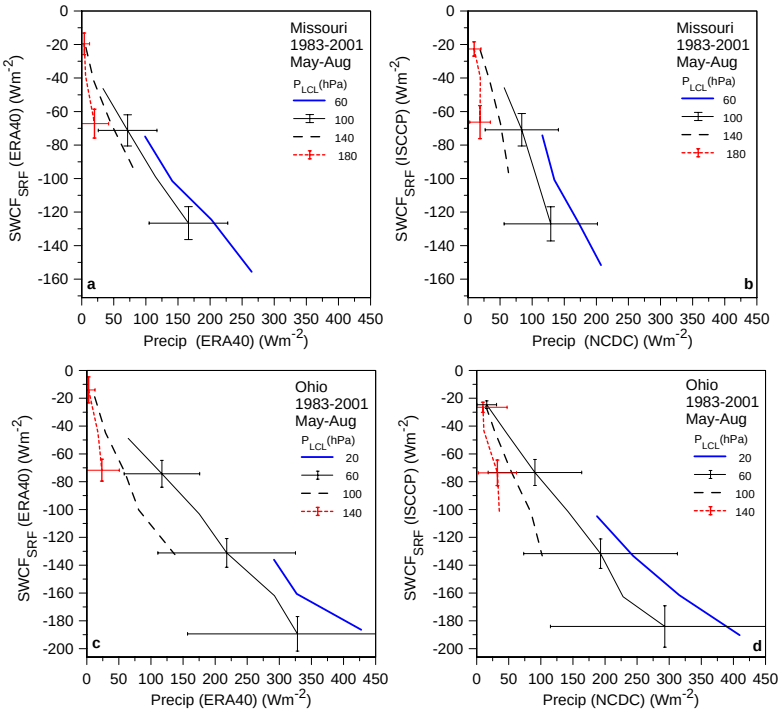

Figure 15. Relationship between precipitation diabatic forcing and surface cloud forcing, stratified by α_{cloud} and P_{LCL} for ERA40 and observations.

the reanalysis and the observations are very similar. For example, for the Ohio basin for P_{LCL}= 60hPa, the ratio ($SWCF_{SRF}$)/Precip ≈0.51 for both reanalysis and ≈0.61 for observations. For the Missouri basin, this same ratio is also larger for the observations (≈0.7) than the reanalysis (≈0.48). This ratio of the diabatic impact of clouds at the surface to that in the atmosphere is an important climate parameter, and it appears that ERA40 has a low bias in summer (and a larger low bias in winter, not shown here). The surface cloud radiative forcing also plays an dominant role in the variation of surface net radiation, R_{netSRF} (see next section).

5. Links between cloud albedo, soil moisture and surface energy budget

The reanalysis data can give some insight into how well the surface energy budget (SEB) might be constrained by satellite observations. The SEB can be divided conceptually into the surface net radiation, R_{netSRF}, and evaporative fraction, EF, defined as

$$EF = \lambda E/(H + \lambda E) \qquad (13)$$

where H and λE are the surface sensible and latent heat fluxes.

5.1 Surface net radiation

The partition of net radiation into clear sky flux and cloud forcing

$$R_{netSRF} = R_{netSRF}(clear) + CF_{SRF} \qquad (14)$$

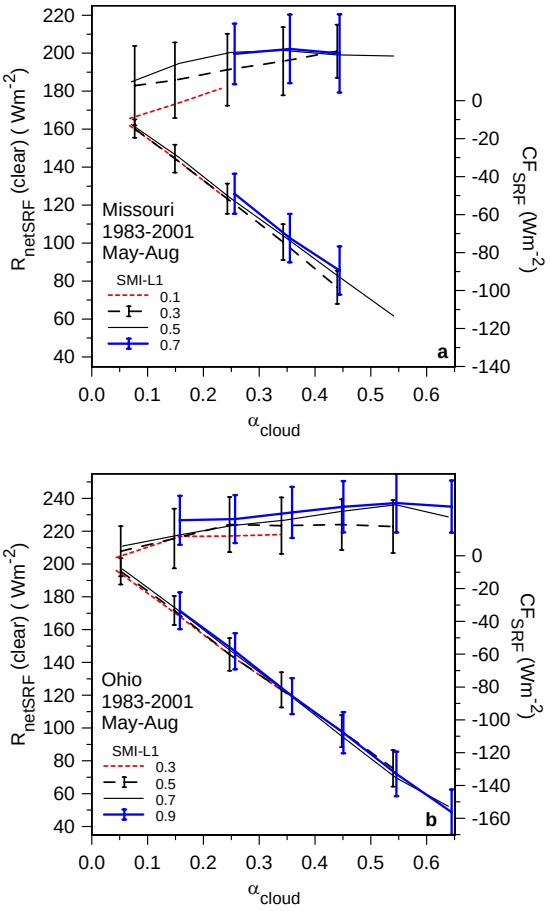

Figure 16. ERA40 surface clear-sky net radiation and cloud forcing as a function of α_{cloud} and SMI-L1 for Missouri and Ohio.

is shown in Figure 16, as a function of α_{cloud} and SMI-L1. The clear-sky flux decreases slightly with drier soils and less cloud cover, while cloud forcing is almost a linear decreasing function of α_{cloud} (as already seen in Figure 14(b) for the P_{LCL} partition). So the variation of R_{netSRF} is dominated by the cloud radiative forcing, which in turn depends on α_{cloud}, which is related to α_{TOA}, as shown in Figure 3.

5.2 Surface fluxes and evaporative fraction

Figure 17 shows the relationship of evaporative fraction EF, to temperature and soil moisture index. As expected, EF increases sharply with SMI, because λE increases and H decreases, and also with temperature. Note that for the Ohio, soil moisture values, EF and the standard deviations are larger than for the Missouri river basin. For reference, Figure 17 also shows the slope with temperature of the classic 'equilibrium evaporation' relation [*Priestley and Taylor* 1972; *McNaughton* 1976], defined as

Equilibrium evaporation = $\beta/(1+\beta)$ (15)

where $\beta = (L/C_p)\,(\partial q_s/\partial T)_p$ is related to the slope of the Clausius-Clapyron equation at constant pressure, taken here as the mean surface pressure, 900hPa for the Missouri and 976hPa for the Ohio. The relations for EF are similar for the two basins, despite the differences in the model vegetation parameters; the Ohio is over 85% forested, while the Missouri forest cover is less than

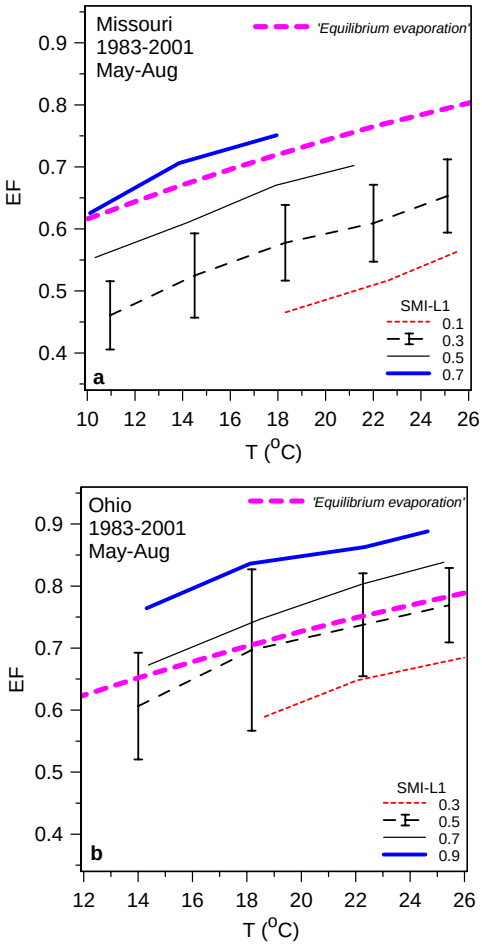

Figure 17. ERA40 EF as a function of temperature and soil moisture index for Missouri and Ohio.

15%. The rather sharp partition of daily mean EF by near-surface (0-7cm) soil moisture in ERA40 would suggest that useful information on EF might be determined from temperature and microwave estimates of near-surface soil water. The more detailed dependence of EF on vegetation characteristics has not been addressed here.

6. Discussion and conclusions

This paper maps the complex relationships in ERA40 of clouds and precipitation to moisture convergence and land surface and boundary layer processes for sub-basins of the Mississippi on time scales of a day and space scales of order 800km. The intent is to provide a framework for model diagnostics that can be evaluated against observations. Model shortwave fluxes have been compared with ISCCP data, and model precipitation with gridded surface observations. Soil moisture, LCL and moisture convergence have been taken from the reanalysis to stratify relationships.

The effective cloud albedo at the surface, defined in terms of the surface SW cloud forcing, is proposed as a useful missing link that connects the cloud fields to both surface and large-scale processes. This definition removes the large seasonal variation of clear-sky fluxes associated with changing solar zenith angle. The surface cloud albedo is closely related to the TOA SW cloud forcing, which is readily observed from space. On the daily timescale, basin-mean cloud albedo for ERA40 and ISCCP are well correlated. However, ERA40 has a systematic low bias in cloud albedo compared to ISCCP for all basins: small in summer, and largest in winter when it reaches -10%. This winter low cloud bias, which is seen on almost all days, suggests that the removal of cloud water by large-scale precipitation processes is too efficient in ERA40. This cloud albedo bias on the basin scale, derived here from satellite data, has almost the same seasonal pattern as that

derived by comparing ERA40 with direct measurements from three flux towers in central Saskatchewan [*Betts et al.* 2006a]. The seasonal bias in model cloud is not related to the seasonal bias in model precipitation, which varies between basins.

In the warm season, cloud albedo and precipitation both increase with moisture convergence and a lower cloud-base in a similar manner in both reanalysis and observations. In ERA40, cloud albedo and precipitation both increase also with moisture convergence and soil moisture. The soil moisture-atmosphere coupling in ERA40 is a two-way interaction. Near-surface relative humidity, the lifting condensation level, soil moisture and precipitation are also closely coupled. Soil moisture, especially in the upper soil layer responds directly to precipitation. Evaporation from the surface increases with increasing soil moisture (as well as when there is water in the skin reservoirs) and this increases RH and lowers the LCL. In addition the evaporation of falling precipitation lowers the LCL by bringing the sub-cloud layer closer to saturation, and this effect increases with increasing precipitation rate.

The relation of precipitation to cloud albedo is similar for both model and observations, with little dependence on moisture convergence, but a strong dependence on cloud-base. The ratio of the surface cloud radiative forcing to the diabatic precipitation heating (of importance to the model climate over land) depends on cloud base, and is lower in ERA40 than for the observations.

The surface energy budget was split into the surface net radiation and the evaporative fraction. The surface net radiation depends on the clear-sky fluxes and the surface cloud radiative forcing, which depends largely on the cloud albedo. Evaporative fraction is closely linked in ERA40 to temperature and soil water (as well as vegetation parameters). This would suggest that useful information on EF might be determined from temperature and microwave estimates of near-surface soil water.

Since cloud feedbacks are a major source of uncertainty in climate modeling, a quantitative framework for their evaluation in relation to both the surface energy budget and the precipitation diabatic forcing is likely to prove useful.

Acknowledgments. Alan Betts acknowledges support from NSF under Grant ATM0529797, from NASA under NEWS Grant NNG05GQ88A and from ECMWF for travel. I am grateful to Anton Beljaars and Pedro Viterbo for helpful discussions and to the entire ERA40 team for their assistance. Especial thanks to Bill Rossow and Y.-C Chang for the basin-averaged ISCCP data; and to Mike Bosilovich for the basin averaged precipitation data, derived from the US Unified Precipitation data provided by the NOAA-CIRES Climate Diagnostics Center, available from http://www.cdc.noaa.gov/.

References

Betts, A.K (1997), 'The Parameterization of deep convection', Chapter 10 (pp 255-279) in "*The Physics and Parameterization of Moist Atmospheric Convection*, Ed. R. K. Smith, NATO ASI Series C: Vol. **505**, Kluwer Academic Publishers, Dordrecht, 498pp.

Betts, A. K. (2004), Understanding Hydrometeorology using global models. *Bull. Amer. Meteorol. Soc*., **85**, 1673-1688.

Betts, A. K., J.H. Ball, A.C.M. Beljaars, M.J. Miller and P. Viterbo (1996), The land-surface-atmosphere interaction: a review based on observational and global modeling perspectives. *J. Geophys. Res.* **101**, 7209-7225.

Betts, A. K., J. H. Ball, M. Bosilovich, P. Viterbo, Y.-C. Zhang, and W. B. Rossow (2003a), Intercomparison of Water and Energy Budgets for five Mississippi Sub-basins between ECMWF

Reanalysis (ERA-40) and NASA-DAO fvGCM for 1990-1999. *J. Geophys. Res*., **108** (D16), 8618, doi:10.1029/2002JD003127.

Betts, A. K., J. H. Ball and P. Viterbo (2003b), Evaluation of the ERA-40 surface water budget and surface temperature for the Mackenzie River basin. *J. Hydrometeorology*, **4**, 1194-1211.

Betts, A. K and P. Viterbo (2005), Land-surface, boundary layer and cloud-field coupling over the south-western Amazon in ERA-40. *J. Geophys. Res*., **110**, D14108, doi:10.1029/2004JD005702.

Betts, A. K, J.H., Ball, P. Viterbo, A. Dai and J. A. Marengo (2005), Hydrometeorology of the Amazon in ERA-40. *J. Hydrometeorology*. **6**, 764-774.

Betts, A. K. (2006), Radiative scaling of the nocturnal boundary layer and the diurnal temperature range, *J. Geophys. Res*., 111, D07105, doi:10.1029/2005JD006560.

Betts, A.K., J. Ball, A. Barr, T. A. Black, J. H. McCaughey and P. Viterbo, (2006a), Assessing land-surface-atmosphere coupling in the ERA-40 reanalysis with boreal forest data. *Agricultural and Forest Meteorology*, doi:10.1016/j.agrformet.2006.08.009.

Betts, A.K., M. Zhao, P. A. Dirmeyer and A.C.M. Beljaars (2006b), Comparison of ERA40 and NCEP/DOE near-surface datasets with other ISLSCP-II datasets. *J. Geophys. Res*., 111, D22S04, doi:10.1029/2006JD007174.

Higgins, R. W., J. E. Janowiak and Y-P. Yao (1996), A Gridded Hourly Precipitation Data Base for the United States (1963-1993), NCEP/Climate Prediction Center ATLAS No. 1, U. S. Department of Commerce, National Oceanic and Atmospheric Administration, National Weather Service.

Higgins, R. W., W. Shi, E. Yarosh, R.Joyce (2000), Improved United States Precipitation Quality Control System and Analysis", NCEP/Climate Prediction Center ATLAS No. 7, U. S. Department of Commerce, National Oceanic and Atmospheric Administration, National Weather Service.

Kållberg, P., A. Simmons, S. Uppala and M. Fuentes (2004), The ERA-40 archive. ERA-40

Project Report, No. 17, 31pp., ECMWF, Shinfield Park, Reading RG2 9AX, UK. http://www.ecmwf.int/publications/library/ecpublications/_pdf/era40/ERA40_PRS17.pdf

McNaughton, K. G. (1976), Evaporation and Advection I: Evaporation from Extensive Homogeneous Surfaces, *Quart. J. Roy. Meteorol. Soc. 102,* 181-191.

Pinker, R. T and 13 co-authors (2003), Surface radiation budgets in support of the GEWEX Continental-Scale International Project (GCIP) and the GEWEX Americas Prediction Project (GAPP), including the North American Land Data Assimilation System (NLDAS) project, *J. Geophys. Res., 108* (D22), doi:10.1029/2002JD003301.

Rossow, W.B., and Y-C. Zhang (1995), Calculation of surface and top-of-atmosphere radiative fluxes from physical quantities based on ISCCP, Part II: Validation and first results. *J. Geophys. Res., 100*, 1167-1197.

Priestley, C. H. B. and Taylor, R. J. (1972), On the Assessment of Surface Heat Flux and Evaporation, *Mon. Wea. Rev. 106*, 81-92.

Uppala, S.M. and 45 co-authors (2005), The ERA-40 Reanalysis. *Quart. J. Roy. Meteorol. Soc, 131*, 2961-3012.

Van den Hurk, B.J.J.M., P. Viterbo, A.C.M. Beljaars and A. K. Betts (2000), Offline validation of the ERA-40 surface scheme. ECMWF Tech Memo, 295, 43 pp., Eur. Cent. For Medium-Range Weather Forecasts, Shinfield Park, Reading RG2 9AX, England, UK.
http://www.ecmwf.int/publications/library/ecpublications/_pdf/tm/001-300/tm295.pdf

Zhang, Y-C., W.B. Rossow, and A.A. Lacis (1995), Calculation of surface and top-of-atmosphere radiative fluxes from physical quantities based on ISCCP, Part I: Method and sensitivity to input data uncertainties. *J. Geophys. Res., 100,* 1149-1165.